

A critical comparison of the Lomb-Scargle and the classical periodograms

Roberto Vio,^{1*} P. Andreani,²

¹Chip Computers Consulting s.r.l., Viale Don L. Sturzo 82, S.Liberale di Marcon, 30020 Venice, Italy

²ESO, Karl Schwarzschild strasse 2, 85748 Garching, Germany

Accepted XXX. Received YYY; in original form ZZZ

ABSTRACT

The detection of signals hidden in noise is one of the oldest and common problems in astronomy. Various solutions have been proposed in the past such as the parametric approaches based on the least-squares fit of theoretical templates or the non-parametric techniques as the phase-folding method. Most of them, however, are suited only for signals with specific time evolution. For generic signals the spectral approach based on the periodogram is potentially the most effective. In astronomy the main problem in working with the periodogram is that often the sampling of the signals is irregular. This complicates its efficient computation (the fast Fourier transform cannot be directly used) but overall the determination of its statistical characteristics. The Lomb-Scargle periodogram (LSP) provides a solution to this last important issue, but its main drawback is the assumption of a very specific model of the data which is not correct for most of the practical applications. These issues are not always considered in literature with theoretical and practical consequences of no easy solution. Moreover, apart from pathological samplings, it is common believe that the LSP and the classical periodogram (CP) usually provide almost identical results. In general, this is true but here it is shown that there are situations where the LSP is less effective than the CP in the detection of signals in noise. There are no compelling reasons, therefore, to use the LSP instead of the CP which is directly connected to the correlation function of the observed signal with the sinusoidal functions at the various frequencies of interest.

Key words: Methods: Statistical – Methods: Data Analysis – Methods: Numerical

1 INTRODUCTION

The detection of weak signals in noise requires a careful analysis of the data with appropriate statistical tools. Given its simple use, one of the most popular approaches is the spectral analysis of the time series by means of the periodogram. In astronomical applications the use of this technique is not straightforward. In fact, from the statistical point of view this tool performs at its best only when the signals are sampled on a regular time grid, an uncommon situation in many astronomical observations. The analysis of a periodogram in the case of irregular sampling is limited by the possibility to fix completely its statistical properties. This problem is not new (e.g. see [Gottlieb et al. 1975](#)) and there have been many attempts to solve it. The solution found in the Lomb-Scargle periodogram (LSP) approach ([Lomb 1976](#); [Scargle 1982](#)) comes at the price of theoretical difficulties which make its use not obvious. In particular, the value of the LSP at a given frequency corresponds to what can be obtained by means of the least-squares fit of a single sine function with the same frequency ([Scargle 1982](#)). This implies that the LSP is equivalent to a least-square fit of a temporal series

using only a specific sine function at a time, i.e. it does not perform a simultaneous fit over the sine functions corresponding to all the inspected frequencies as it should be necessary. However, only in the case of even samplings and in correspondence to the Fourier frequencies a set of sine functions constitutes an orthonormal basis and only in this case the fit of a single sine function provides the same result as the simultaneous fit of the entire set of sine functions (e.g. see [Hamming 1973](#), p. 450). This does not happen for uneven samplings. As a consequence the LSP it is not based on the correct least-squares model (see appendix A for a formalized explanation). Therefore, the real effectiveness and reliability of the implicit operation at the basis of the LSP is not founded on a correct ground.

Over the years many papers have been dedicated to understand and resolve the shortcomings of the LSP as, for example, the impossibility to describe it in terms of the spectral window, the development of specific computer codes, or the fact that, contrary to the even sampling case, the effect of the mean value of the signals is not limited to the zero frequency (some recent works are [Reegen 2007](#); [Zechmeister & KÄijrster 2009](#); [Vio et al. 2010, 2013](#); [VanderPlas 2018](#), and reference therein). However, an overlooked point is that ,although in the case of signals constituted only by noise the two periodograms provide almost identical results, the same may be

* robertovio@tin.it

not true if the searched signal is present. The consequence is that the two approaches provide different statistical significance to the presence of a signal in a given time series. There are no compelling theoretical arguments that impose the use of the LSP instead of the classical periodogram (CP). Indeed, this last is directly connected to the correlation function of the observed signal with the sinusoidal functions at the various frequencies of interest and hence provides a direct estimate of the power spectrum avoiding the modeling of the data. This is even more true since, as it will be shown below, there are situations where the LSP is less effective than the CP in the detection of signals in noise.

In Sect. 2 we discuss the limitations of the LSP and in Sect. 3 we describe the statistical characteristics of the entries of the CP. In Sect. 4 the characteristics of the LSP and the CP are compared and tested in Sect. 5 with some numerical experiments, whereas in Sect. 6 an experimental signal is outlined. Finally, Sect. 7 summarizes our conclusions. For ease of reading three appendices have been added which contain most of the mathematics used in Sects. 2, 4, and 5.

2 MATHEMATICS OF THE PROBLEM

When a continuous signal $x(t)$ is sampled on an irregular time grid $[t_0, t_1, \dots, t_{M-1}]$, a time series $[x_{t_0}, x_{t_1}, \dots, x_{t_{M-1}}]$ is obtained. The CP of $\{x_{t_i}\}$ at a given frequency ν is defined as

$$p_\nu = a_\nu^2 + b_\nu^2 \quad (1)$$

where

$$a_\nu = \frac{1}{\sqrt{M}} \sum_{i=0}^{M-1} x_{t_i} \cos 2\pi\nu t_i, \quad (2)$$

$$b_\nu = \frac{1}{\sqrt{M}} \sum_{i=0}^{M-1} x_{t_i} \sin 2\pi\nu t_i. \quad (3)$$

The function p_ν can be interpreted as the correlation between the time series and the sine and cosine modes with frequency ν . It provides a statistical measure of the similarity between the time series and a discrete sinusoidal signal of frequency ν . Hence, a high peak in p_ν is indicative of the presence of a sinusoidal component of frequency ν in $\{x_{t_i}\}$. For this reason, the periodogram is typically used to test whether a time series contains the contribution of a deterministic signal $\{s_{t_i}\}$ or it is constituted by a noise $\{n_{t_i}\}$ only, i.e. to decide between the hypotheses $x_{t_i} = s_{t_i} + n_{t_i}$ and $x_{t_i} = n_{t_i}$.

In the case of a regular sampling time grid, i.e. $t_0 = 0, t_1 = 1, \dots, t_{M-1} = M - 1$, the question is relatively simple if the periodogram is computed in correspondence to the so called Fourier frequencies, i.e. $\nu_k = k/(M - 1)$, $k = 0, 1, \dots, M - 1$. Indeed, under the hypothesis $x_i = n_i$, $i = 0, 1, \dots, M - 1$, with n_i a zero-mean, Gaussian, stationary, white-noise process with standard deviation σ_n , it can be verified that, independently of k , the normalized version $p_k/\sigma_n^2 \rightarrow p_k$ is given by the sum of two squared independent, zero-mean, Gaussian, random quantities with variance equal to $1/2$. As a consequence, the corresponding probability density function (PDF) is the exponential distribution (Scargle 1982),

$$g_{P_k}(p_k) = \exp(-p_k), \quad (4)$$

with cumulative distribution function (CDF),

$$G_{P_k}(p_k) = 1 - \exp(-p_k). \quad (5)$$

Hence, the probability of false alarm (PFA), that is the probability

α with which at a generic frequency p_k is expected to exceed by chance a level z , is

$$\alpha = 1 - G_{P_k}(z); \quad (6)$$

$$= 1 - (1 - e^{-z}). \quad (7)$$

However, if we consider all the frequencies of the periodogram, the probability α that one among them exceeds by chance a level z is

$$\alpha = 1 - G_{P_k}^{N^*}(z); \quad (8)$$

$$= 1 - (1 - e^{-z})^{N^*}, \quad (9)$$

with N^* the number of statistically independent frequencies. Considering that whenever $k \neq k'$, with $k, k' = 0, 1, \dots, M/2$, p_k is independent of $p_{k'}$, in the present case it is $N^* = M/2$. We call the probability α given by Eqs. (8) and (9) the specific (to the considered frequency) probability of false alarm (SPFA). Using the SPFA it is possible to fix a detection threshold,

$$L_{\text{Fa}} = -\ln[1 - (1 - \alpha)^{1/N^*}] \quad (10)$$

which is called the ‘‘level of false alarm’’. Without loss of generality, here and henceforth σ_n will be taken to be unity¹.

When the sampling is irregular, the situation becomes more complex given that a_ν and b_ν are zero-mean, Gaussian, random quantities but in this case correlated and with different variances. Hence, for a fixed frequency, the PDF of p_ν is not given by $g_{P_\nu}(p_\nu)$. Scargle (1982) bypasses this problem introducing a modified version \hat{p}_ν of the CP,

$$\hat{p}_\nu = \frac{1}{2}(\hat{a}_\nu^2 + \hat{b}_\nu^2), \quad (11)$$

where

$$\hat{a}_\nu = \frac{\sum_{i=0}^{M-1} x_{t_i} \cos [2\pi\nu(t_i - \tau)]}{\sqrt{\sum_{i=0}^{M-1} \cos^2 [2\pi\nu(t_i - \tau)]}}, \quad (12)$$

$$\hat{b}_\nu = \frac{\sum_{i=0}^{M-1} x_{t_i} \sin [2\pi\nu(t_i - \tau)]}{\sqrt{\sum_{i=0}^{M-1} \sin^2 [2\pi\nu(t_i - \tau)]}}, \quad (13)$$

with τ defined by

$$\tan(4\pi\nu\tau) = \frac{\sum_{i=0}^{M-1} \sin(4\pi\nu t_i)}{\sum_{i=0}^{M-1} \cos(4\pi\nu t_i)}. \quad (14)$$

The reason for such a modification is that, under the hypothesis $x_{t_i} = n_{t_i}$, \hat{a}_ν and \hat{b}_ν are zero-mean, unit variance, uncorrelated, Gaussian, random quantities. Therefore, the PDF of \hat{p}_ν is again of exponential type.

A further problem which raises in the case of irregular sampling is that it is no longer possible to define a set of natural frequencies on which to compute the periodogram such as the Fourier frequencies which permit the reconstruction of the signal via the discrete inverse Fourier transform. Hence, there is no reason why the number N of frequencies where to compute \hat{p}_ν must be equal to the number M of the sampling time instants. Indeed, often $N \gg M$. Here, the point is that the number N^* of independent frequencies is not defined and the threshold L_{Fa} as given by Eq. (10) is not computable. An analysis of this subject is available in Home & Baliunas (1986) and VanderPlas (2018) and references therein. However, as discussed in Press et al. (1992), the exact value of N^* is not critical.

¹ This can be obtained by standardize the time series to unit-variance, i.e. $x_i \rightarrow x_i/\sigma_n$

Anyway, in the case of a semi-regular sampling and a regular frequency grid with step equal to $1/\Delta t$, with Δt the smallest time step of the sampling, $N^* = M/2$ represents a reasonable choice (e.g. see Vio et al. 2010, 2013). With random sampling patterns $N^* = M$ may be an appropriate choice (Press et al. 1992). A more precise, although computationally expensive, estimation of N^* can be obtained from the rank of the correlation matrix Σ of the periodogram entries (see appendix B). Recently, an alternative technique based on the extreme value theory has been proposed by Baluev (2008, 2014) (see also Süveges 2014; Süveges et al. 2015).

From the discussion above, it could be derived that with the LSP the computational issue of the PFA has been exactly solved, but in reality this is not the case. Equations (12) and (13) represent a local operation, i.e. an operation which is applied only on a frequency at a time and using specific normalization coefficients for that frequency, it does not use the data related to the remaining frequencies of interest and hence it operates differently at different frequencies. The consequence is that \hat{p}_v represents a distorted version of p_v . From both the theoretical and practical points of view this is not desirable and may give rise to unexpected consequences. In particular, as shown in Sect. 3, each entry of the CP has its own PDF $f_{p_v}(p_v)$ and CDF $F_{p_v}(p_v)$ which are different for different frequencies. When p_v is converted into \hat{p}_v , in general it results that $G_{\hat{p}_v}(\hat{p}_v) \neq F_{p_v}(p_v)$. Hence, the same holds for the corresponding PFAs (see below). Given that the LSP is computed through a procedure that distorts the CP and, as seen above, it is not based on a correct least-squares model, there is no reason why the outgoing PFAs should be preferred to those produced by the CP which is directly connected to the correlation function of the observed signal x with the sinusoidal functions at the various frequencies of interest.

3 STATISTICAL CHARACTERISTICS OF THE ENTRIES OF THE CLASSICAL PERIODOGRAM

The PDF $f_{p_v}(p_v)$ of $p(v)$ is equivalent to the PDF $f_Z(z)$ of the random variable $Z = X_1^2 + X_2^2$ with X_1 and X_2 zero-mean, Gaussian, random variables with standard deviation σ_1 and σ_2 , respectively, and correlation coefficient ρ . This PDF is given by (Simon 2006, see also appendix C for a slightly different form best suited for implementation)

$$f_Z(z) = \frac{1}{2\sigma_1\sigma_2\sqrt{1-\rho^2}} \exp\left[-\frac{1}{4}(\beta^+ - \gamma^+)z\right] I_0\left(\frac{1}{4}\gamma^+z\right), \quad (15)$$

with $z \geq 0$,

$$\gamma^+ = \frac{[(\sigma_1^2 + \sigma_2^2)^2 - 4\sigma_1^2\sigma_2^2(1-\rho^2)]^{1/2}}{\sigma_1^2\sigma_2^2(1-\rho^2)}, \quad (16)$$

$$\beta^+ = \gamma^+ + \frac{\sigma_1^2 + \sigma_2^2}{\sigma_1^2\sigma_2^2(1-\rho^2)}, \quad (17)$$

and $I_0(\cdot)$ the modified Bessel function of the first kind of zero order.

The corresponding central moments are given by ²

$$E\left[(Z - \bar{Z})^k\right] = \sum_{i=0}^k \frac{k!}{i!(k-i)!} E[Z^i]. \quad (18)$$

² Symbol $E[\cdot]$ denotes the expectation operator.

where $E[Z^k]$

$$E[Z^k] = \frac{2^{2k+1}k!}{\sigma_1\sigma_2\sqrt{1-\rho^2}(\beta^+ - \gamma^+)^{k+1}} \times {}_2F_1\left[\frac{k+1}{2}, \frac{k}{2} + 1; 1; \left(\frac{\gamma^+}{\beta^+ - \gamma^+}\right)^2\right], \quad (19)$$

with ${}_2F_1(\cdot, \cdot; \cdot; \cdot)$ the Gauss hypergeometric function. Cases of interest are $k = 1$ and 2 for which

$${}_2F_1\left[\frac{k+1}{2}, \frac{k}{2} + 1; 1; x\right] = \begin{cases} \frac{1}{(1-x)^{3/2}} & \text{if } k = 1, \\ \frac{2+x}{2(1-x)^{5/2}} & \text{if } k = 2. \end{cases} \quad (20)$$

The corresponding cumulative distribution function $F_Z(z)$ is

$$F_Z(z) = 1 + \exp\left[-\frac{1}{4}(\beta^+ - \gamma^+)z\right] I_0\left(\frac{1}{4}\gamma^+z\right) - 2Q_1(A, B), \quad (21)$$

where $Q_1(\cdot, \cdot)$ is the Marcum Q-function with

$$A = \frac{\sqrt{\sigma_1^2 + \sigma_2^2 - 2\sigma_1\sigma_2\sqrt{1-\rho^2}}}{2\sigma_1\sigma_2\sqrt{1-\rho^2}} \sqrt{z}; \quad (22)$$

$$B = \frac{\sqrt{\sigma_1^2 + \sigma_2^2 + 2\sigma_1\sigma_2\sqrt{1-\rho^2}}}{2\sigma_1\sigma_2\sqrt{1-\rho^2}} \sqrt{z}. \quad (23)$$

At first sight these functions could appear rather convoluted, but they are commonly used in statistics and engineering (e.g. see Helstrom 1968; Van Trees 2001; Shankar 2017) and indeed they may be found in all main software packages.

In the present case, it is $z = p_v$, $\sigma_1 = \sigma_{a_v}$, $\sigma_2 = \sigma_{b_v}$, $\rho = \rho_v$ with

$$\sigma_{a_v}^2 = \frac{1}{M} \sum_{i=0}^{M-1} \cos^2(2\pi v t_i), \quad (24)$$

$$\sigma_{b_v}^2 = \frac{1}{M} \sum_{i=0}^{M-1} \sin^2(2\pi v t_i), \quad (25)$$

and (Vio et al. 2013)

$$\rho_v = \frac{E[a_v b_v]}{\sigma_{a_v} \sigma_{b_v}} = \frac{\sum_{i=0}^{M-1} \sin(4\pi v t_i)}{2\sqrt{\sum_{i=0}^{M-1} \cos^2(2\pi v t_i)} \sqrt{\sum_{i=0}^{M-1} \sin^2(2\pi v t_i)}}. \quad (26)$$

The PDF $f_{p_v}(p_v)$ and the CDF $F_{p_v}(p_v)$ permit a spectral analysis of the time series based on the CP.

4 CLASSICAL VS. THE LOMB-SCARGLE PERIODOGRAM

There are various reasons why working with the CP is more advantageous than with the LSP. First, with $f_{p_v}(p_v)$ and $F_{p_v}(p_v)$ the computation of the statistical significance of a peak in the periodogram does not require that this last is modified frequency by frequency as it happens if Eqs. (12) and (13) are used. This makes the detection procedure more transparent and intuitive. Second, the CP does not require specific software for its implementation. Nonuniform fast Fourier transform algorithms are already widely available (Bagchi & Mitra 1999; Potts et al. 2001). Moreover, as shown in Vio et al. (2013), if the time series are rebinned into a sufficiently high number of equispaced bins, the periodogram can be computed with arbitrary accuracy by means of the standard fast Fourier transform,

with obvious computational gains. Finally, the computation of the spectral window $w(\nu)$ does not present particular difficulties while, strictly speaking, it cannot be computed in the context of the LSP method. This is because, as seen above, the decorrelation of the coefficients a_ν and b_ν is a local operation, hence the mutual relationship among the various frequencies in \hat{p}_ν is altered. We recall that the spectral window, defined as

$$w(\nu) = \left| \sum_{i=0}^{M-1} e^{-i2\pi\nu t_i} \right|^2, \quad (27)$$

with $\iota = \sqrt{-1}$, is key since all spectral leakage effects (aliasing, sidelobes, interference phenomena, ghosts, etc.) are manifested directly in it and can be easily evaluated quantitatively (Deeming 1975; Scargle 1982).

With the CP, however, the detection threshold cannot be obtained in analytical form. Therefore, in the case it is necessary to test the statistical significance of a peak at a prefixed frequency (e.g. when it is known a priori that if a periodic signal of interest is present in a time series it contributes to the periodogram at a specific frequency) the detection threshold must be numerically computed by solving the equation

$$1 - F_{P_\nu}(L_{Fa}) = \alpha \quad (28)$$

for L_{Fa} . However, since $F_{P_\nu}(p_\nu)$ is a monotone increasing function, its computation is not difficult. An effective alternative is to fix a threshold value α for the PFA, to compute the quantities $\{\alpha'_i\}$ for the peak of interest $\{p_{\nu_i}^*\}$,

$$\alpha'_i = 1 - F_{P_\nu}(p_{\nu_i}^*), \quad (29)$$

and then to claim the peak as statistically significant if $\alpha'_i \leq \alpha$.

When the frequencies where the contribution of a signal takes place are unknown, it is common practice to test the statistical significance of the highest peak z_{\max} in the spectrogram. However, its SPFA cannot be computed on the basis of the method used to obtain Eq. (9) since each entry of p_ν has its own PDF. This is the main reason at the basis of the LSP where all entries are forced to follow the same exponential distribution. Only in this way the SPFA can be estimated by means of Eq. (9) or the technique by Baluev (2008, 2014). A possible approach to avoid this issue is based on the fact that in most cases of interest the coefficients a_ν and b_ν are almost uncorrelated for the vast majority of the frequencies (Scargle 1982; Vio et al. 2010, 2013). Hence, their PDFs are expected to be similar and then the SPFA corresponding to z_{\max} can be computed on the basis of

$$\alpha = 1 - \bar{F}_{Z_{\max}}^{N^*}(z_{\max}), \quad (30)$$

where the CDF $\bar{F}_{P_\nu}(p_\nu)$, with PDF $\bar{f}_{P_\nu}(p_\nu)$, is given by Eq. (21) with σ_{a_ν} , σ_{b_ν} and ρ_ν substituted, respectively, by $\bar{\sigma}_a$, $\bar{\sigma}_b$ and $\bar{\rho}$. The first two quantities correspond to the mean values of σ_{a_ν} and σ_{b_ν} evaluated on all the frequencies of the periodogram whereas the last quantity corresponds to the mean value of the absolute values of ρ_ν . Alternatively and more simply, it is possible to exploit the fact that, as shown by Vityazev (1996a,b) on the basis of a theoretical study using the spectral window, the CP is typically almost identical to the LSP. As a consequence, the entries of p_ν are approximately distributed according to the classical exponential PDF. In other words, the SPFA of a peak in p_ν can be estimated on the basis of Eq. (9) exactly as it is done for the LSP. This approach is suggested, although with some caution, also by Baluev (2014, Sect. 4.4).

Here one could ask why do not use directly the LSP. The point

is that, as it is shown in appendix C, when ρ is sufficiently large, $f_Z(z)$ given by Eq. (15) can be well approximated by

$$f_Z(z) \approx \frac{1}{\sqrt{2\pi z}} e^{-z/2}. \quad (31)$$

This function decreases with z slower than the classical exponential distribution. With the LSP approach the entries of the periodogram p_ν are modified and forced to follow the exponential distribution which therefore has a faster right tail decay than $f_{P_\nu}(p_\nu)$. The consequence is that the peaks which in p_ν are related to frequencies characterized by $|\rho_\nu| \gg 0$ in \hat{p}_ν tend to be more lowered than the peaks characterized by $\rho_\nu \approx 0$, i.e. in the LSP the relative heights of the peaks are modified. Such effect becomes important for high values of p_ν . The consequences are potentially harmful since a peak due to a signal well above the level of the noise in the CP can be below the noise level in the LSP (see below for an example). For this reason, if $|\rho_\nu| \approx 0$ for the frequency of the peak of interest, its SPFA can be computed by means of the CP and one of the above mentioned methods. In the improbable case that $|\rho_\nu| \gg 0$ some further validation is necessary (e.g., by means of numerical simulations).

5 NUMERICAL EXAMPLES

Figures 1 and 2 show the relationship between the coefficients a_ν and b_ν at two specific frequencies, as well the corresponding $f_{P_\nu}(p_\nu)$ and $F_{P_\nu}(p_\nu)$, resulting from a numerical experiment where 10^6 realizations of a discrete zero-mean, unit-variance, Gaussian, white-noise process is simulated with sampling time instants given by $t_i = (m \times 5 + j)/205$, $i = j + m/2$ with $j = 1, 2, \dots, 5$, and $m = 0, 2, \dots, 40$. The resulting time series contain 105 data with sampling times in the range $[0, 1]$ where every sequence of five times containing an observation is followed by a sequence of five times with no data. In this way, a time series with periodic gaps is simulated. The sampling time step of the data is $\Delta t = 4.902 \times 10^{-3}$ with corresponding Nyquist frequency $\nu_{Ny} = 102$. In practical applications time series similar to these ones are not very common. However, the perfect regularity of both the sampling and the gap distribution exacerbates certain problems related to the irregular sampling and hence make easier their analysis.

Two frequencies are considered, $\nu = 0.05$ and $\nu = 1.20$. Since the frequency resolution of a periodogram is provided by the inverse of the time span $\Delta T = t_{\max} - t_{\min}$ of the input data (equal to one in the present case), the first frequency corresponds to a sinusoid which is not sampled on a complete cycle. The reason for such a choice is that, as it is visible in top-left panel of Fig. 1, the corresponding coefficients a_ν and b_ν are strongly correlated ($\rho_\nu = 0.85$). For reasons explained below, this is a situation difficult to reproduce with frequencies greater than $1/\Delta T$. Indeed, ρ_ν results much less significant for the frequencies $\nu \geq 1$. An example is given in the top-left panel of Fig. 2 for the frequency $\nu = 1.20$ for which $\rho_\nu = 0.17$.

The top-right and the bottom-left panels of Fig. 1 show that $f_{P_\nu}(p_\nu)$ and $F_{P_\nu}(p_\nu)$ at $\nu = 0.05$ are different from the corresponding exponential counterpart $g_{P_\nu}(p_\nu)$ and $G_{P_\nu}(p_\nu)$, but only the first two are in good agreement with the respective empirical estimators of the PDF and the CDF. The bottom-right panel in the same figure shows that the PFAs provided by the two CDFs are very different. As the corresponding panels in Fig. 2 show, these differences almost disappear for the frequency $\nu = 1.20$.

These results are easy to understand by considering the distribution of the angles $\theta_i = 4\pi\nu t_i$ of a unit circle. Indeed, from

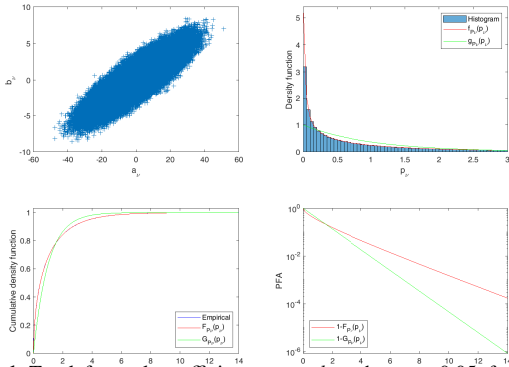


Figure 1. Top-left panel: coefficients a_ν vs. b_ν , when $\nu = 0.05$, for the numerical experiment where 10^6 zero-mean, unit-variance, Gaussian, white-noise processes are simulated on a time sampling grid containing periodic gaps (see the text). Note the strong correlation between these two quantities due to the high values of the correlation coefficient $\rho_\nu = 0.85$. Top-right and bottom-left panel: PDF $f_{p_\nu}(p_\nu)$ and the CDF $F_{p_\nu}(p_\nu)$ of the values of the periodogram $p_\nu = a_\nu^2 + b_\nu^2$. For reference, the exponential PDF $g_{p_\nu}(p_\nu)$ and CDF $G_{p_\nu}(p_\nu)$ are plotted as the histogram and the empirical CDF. The almost perfect overlapping of $f_{p_\nu}(p_\nu)$ and $F_{p_\nu}(p_\nu)$ with the corresponding empirical functions is clear. Indeed, they are indistinguishable in the figures. The same is not true for $g_{\hat{p}_\nu}(\hat{p}_\nu)$ and $G_{\hat{p}_\nu}(\hat{p}_\nu)$. Bottom-right panel: the probability of false alarm $1 - F_{p_\nu}(p_\nu)$ vs. the probability of false alarm $1 - G_{\hat{p}_\nu}(\hat{p}_\nu)$.

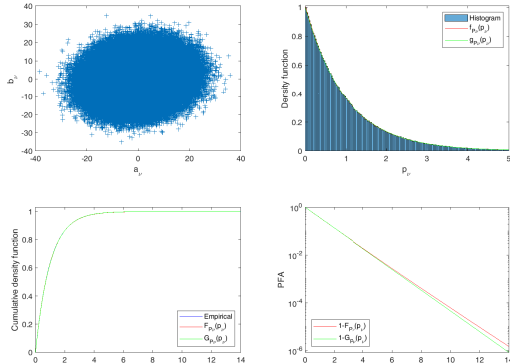


Figure 2. The same as in Fig. 1 but for $\nu = 1.20$. Here, $g_{p_\nu}(p_\nu)$ and $G_{p_\nu}(p_\nu)$ are very similar to $f_{p_\nu}(p_\nu)$ and $F_{p_\nu}(p_\nu)$, respectively. This is the consequence of the small value of the correlation coefficient $\rho_\nu \approx 0$.

Eq. (A2) it results that the correlation ρ_ν between the coefficients a_ν and b_ν at a given frequency ν is proportional to $\sum_{i=0}^{M-1} \sin(4\pi\nu t_i)$. Since the sine function is an odd function, one may expect that $\rho_\nu \approx 0$ if the angles $\{\theta_i\}$ of a unit circle are uniformly and/or symmetrically distributed. This is a very probable situation for the vast majority of the frequencies. Indeed, even if for a given frequency it happens that the angles $\{\theta_i\}$ cluster somewhere on the unit circle, it is quite improbable that such a cluster could survive for the other frequencies (Vio et al. 2013). The different distributions on the unit circle of the angles $\{\alpha_i\}$ corresponding to the two frequencies $\nu = 0.05$ and $\nu = 1.20$ are visible in Fig. 3. It is clear that for the frequency $\nu = 0.05$ the distribution is asymmetric contrary to that corresponding to the frequency $\nu = 1.20$. Similar experiments with other kinds of sampling time grids provide identical results.

The two effects that a high value of ρ_ν can have on \hat{p}_ν , mentioned at the end of Sects. 2 and 4, are visible in Figs. 4-6. In particular, Fig. 4 shows $G_{\hat{p}_\nu}(\hat{p}_\nu)$ vs. $F_{p_\nu}(p_\nu)$ for two frequencies, $\nu = 0.05$ and $\nu = 1.00$, characterized by a correlation coefficient ρ_ν equal to 0.85 and approximately 0, respectively. This experiment is based on the 10^6 time series used above. It is evident that when $|\rho_\nu|$ is small the two CDF's are, as expected, identical. The situation drastically changes for greater values of $|\rho_\nu|$. The result of this exercise is telling us that, as stated above, the PFA and hence the SPFA obtained from the LSP and the CP can be very different for high values of $|\rho_\nu|$.

The second effect is visible in the top panels of Figs. 5 and 6 which show the CP and the LSP (frequency range $[0, 5]$) for the sig-

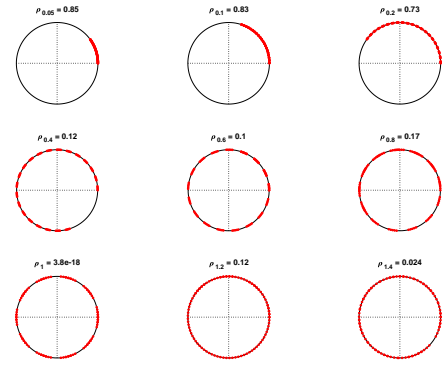


Figure 3. Distribution of the angles $\theta_i = 4\pi\nu t_i$ on the unit circle corresponding to a set of different frequencies ν for the numerical experiments described in the text. The circles corresponding to the frequencies $\nu = 0.05$ and 1.20 are to be related to the results shown in Figs. 1 and 2.

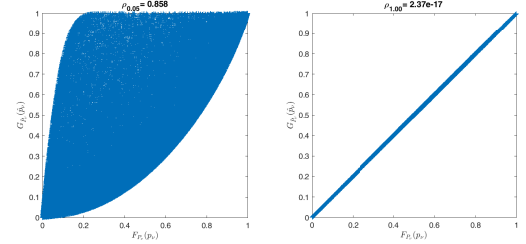


Figure 4. CDF $F_{p_\nu}(p_\nu)$ vs. CDF $G_{\hat{p}_\nu}(\hat{p}_\nu)$ for the 10^6 time series used in the Figs. 1 and 2. Here, the frequencies $\nu = 0.05$ and $\nu = 1.00$ have been used which have ρ_ν equal to 0.85 and approximately 0, respectively. It is evident that, especially for great values of $|\rho_\nu|$, the decorrelation of the coefficients a_ν and b_ν operated by the Lomb-Scargle method alters the statistical characteristics of the periodogram.

nal used in the numerical experiments by Vityazev (1996a) where the signal

$$x(t) = \cos(2\pi\nu_1 t) + \cos(2\pi\nu_2 t) \quad (32)$$

is sampled with periodic gaps. In particular, the sampling time instants are regularly distributed with a constant time interval Δt and to N_o successive observations follow N_m missing points with the group of $N_o + N_m$ points repeated M times. The top panel in Fig. 5 shows the correlation coefficient ρ_ν for the simulation with $\nu_1 = 0.5$, $\nu_2 = 3.3$, $N_o = 3$, $N_m = 7$, $M = 15$ and $\Delta t = 0.1$ where it is visible that, contrary to the frequency ν_2 , the frequency ν_1 is characterized by a $\rho_\nu \gg 0$. The bottom panel in the same figure shows the corresponding LSP and CP. As expected, the amplitude of the peak at the frequency ν_1 in the LSP is smaller than the amplitude of the corresponding peak in the CP. The same does not hold for the peak at the frequency ν_2 . In the experiment of Fig. 6, which simulates observations characterized by a long gap, the signal (32), with $\nu_1 = 0.0625$ and $\nu_2 = 3.3$, is sampled on a time grid with $N_o = 40$, $N_m = 40$, $M = 2$ and $\Delta t = 0.1$. Also here it is $\rho_\nu \gg 0$ for the frequency ν_1 whereas $\rho_\nu \approx 0$ for the frequency ν_2 . Again, it is evident that in the LSP the peak at the frequency ν_1 is lower than the corresponding peak in the CP.

The lowering of the peaks in the LSP can have consequences in the case of noisy signals. This is visible in the top-right panel of Fig. 11 which shows the CP and the LSP (frequency range $[0, 20]$) of a simulated time series with the same characteristics of the signal used in Fig. 4 added to a sinusoidal signal. The amplitude of the sinusoid is 0.15 whereas its frequency is $\nu = 10.2$. This last corresponds to the frequency in the classical periodogram with the greatest ρ_ν (see the top-left panel of the same figure). It is clear that while $\rho_{10.2}$ corresponds to a predominant peak at the frequency of

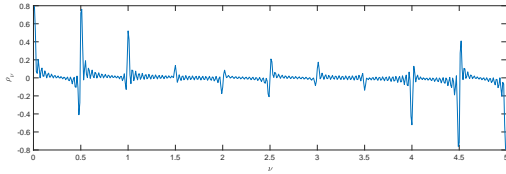


Figure 5. Top panel: Correlation coefficients ρ_ν between the coefficient a_ν and b_ν for the periodogram of a signal $x(t) = \cos(2\pi\nu_1 t) + \cos(2\pi\nu_2 t)$ where the sampling time instants are regularly distributed with a constant time interval Δt and to N_o successive observations follow N_m missing points with the group of $N_o + N_m$ points repeated M times. Here, $\nu_1 = 0.5$, $\nu_2 = 3.3$, $N_o = 3$, $N_m = 7$, $M = 15$ and $\Delta t = 0.1$. Contrary to the frequency ν_2 , the frequency ν_1 corresponds to a frequency of the CP with $\rho_\nu \gg 0$. Bottom panel: corresponding Lomb-Scargle and CP.

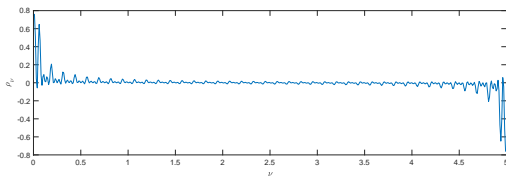
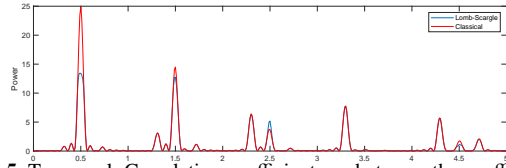
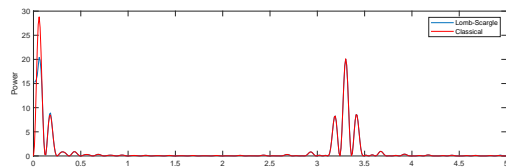


Figure 6. The same as in Fig. 5 but with $\nu_1 = 0.0625$, $\nu_2 = 3.3$, $N_o = 40$, $N_m = 40$, $M = 2$ and $\Delta t = 0.1$. This case correspond to a signal with a sampling characterized by a long gap. Also here, contrary to the frequency ν_2 , the frequency ν_1 corresponds to a frequency of the CP with $\rho_\nu \gg 0$.



the sinusoid, the same is not true for $\hat{p}_{10.2}$. In other words, with the LSP it is not even possible to guess the presence of a signal in the time series. Again, this is the consequence of the above mentioned fact that when $|\rho_\nu| \gg 0$ the PDF $g_{\hat{p}_\nu}(\hat{p}_\nu)$ is more short tailed than $f_{p_\nu}(p_\nu)$. That this is not a conclusion due to a single simulation is supported by the bottom-panel of Fig. 11 which shows the mean of the CPs and of the LSPs obtained from 5000 simulated time series with the same characteristics of the time series used for the top panels. As a countercheck, the same effect is not visible in Fig. 12 where the same experiment is repeated with an amplitude of the sinusoid set again to 0.15 but with a frequency $\nu = 15.0$ for which $\rho_\nu \approx 0$.

The same conclusion is supported by Fig. 7 which shows what happens with the same signal as in the previous experiment when 200 sampling time instants are randomly and uniformly distributed in the interval $[0, 1]$. These kinds of sampling is by far less pathological than the one considered above. From these figures it is evident that $|\rho_\nu| \approx 0$ for all the considered frequencies. Hence, the LSP and the CP are, as expected, very similar. By the way, this is the reason why in practical applications the limitations of the LSP are not apparent.

In order to test the reliability of the SPFA when estimated by means of analytical methods, Figs. 8-10 show the histogram of the values \hat{z}_{\max} and z_{\max} of the highest peak of, respectively, the LSP and the CP obtained from 5000 numerical simulations of a zero-mean, unit-variance white-noise process with the time sampling and the frequency pattern identical, respectively, to the experiments used for Figs. 5, 6 and 11. Three methods has been used to estimate the corresponding analytical PDF. In particular, the PDF $g_{\hat{z}_{\max}}(\hat{z}_{\max})$

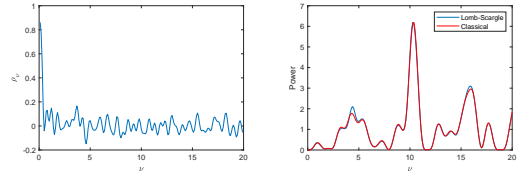


Figure 7. Top-left panel: Correlation coefficients ρ_ν between the coefficient a_ν and b_ν for the periodogram of a zero-mean, unit-variance, Gaussian, white-noise process added with a sinusoidal signal of frequency $\nu = 10.2$ and amplitude set to 0.15. The sampling time grid of the signal is constituted by 200 instants uniformly and randomly distributed in the interval $[0, 1]$. The LSP and the CP are computed on 200 frequencies uniformly distributed in the range $[0, 20]$. Bottom-panel: mean of the Lomb-Scargle and CP obtained from 5000 times series with the same characteristics of the time series used in the top-right panel. To notice also in this case that, since $\rho_\nu \approx 0$ for all the frequencies, the Lomb-Scargle and the CP are very similar.

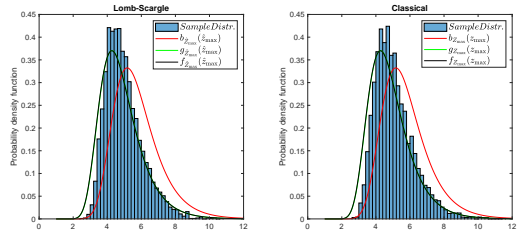
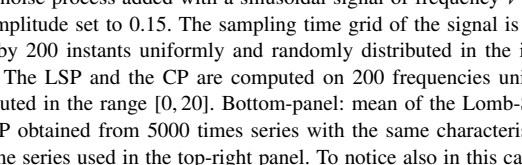
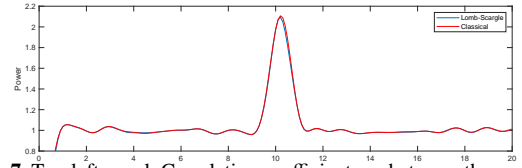


Figure 8. Histogram of the greatest peak for both the LSP and the CP obtained from 5000 numerical simulations of the experiment in Fig. 5 when the time series contains only a zero-mean, unit-variance white noise. The PDF $b_{\hat{z}_{\max}}(\hat{z}_{\max})$ derived from the extreme value theory by Baluev (2008), the PDF $g_{\hat{z}_{\max}}(\hat{z}_{\max})$ based on the exponential distribution given by Eq. (33) and the proposed PDF $\hat{f}_{z_{\max}}(z_{\max})$ given by Eq. (34) are also plotted.

corresponding to the CDF $G_{z_{\max}}^{N^*}(\hat{z}_{\max})$ given in Eq. (8)

$$g_{\hat{z}_{\max}}(\hat{z}_{\max}) = N^* e^{-\hat{z}_{\max}} (1 - e^{-\hat{z}_{\max}})^{N^*-1}, \quad (33)$$

the PDF $\hat{f}_{z_{\max}}(z_{\max})$ corresponding to the CDF $F_{z_{\max}}^{N^*}(z_{\max})$ in Eq. (30)

$$\hat{f}_{z_{\max}}(z_{\max}) = N^* \bar{F}_{z_{\max}}(z_{\max}) \bar{F}_{z_{\max}}^{N^*-1}(z_{\max}), \quad (34)$$

where N^* is computed via the method presented in appendix B, and the PDF $b_{\hat{z}_{\max}}(\hat{z}_{\max})$ derived from the extreme value theory by Baluev (2008).

From these figure it is possible to derive the following. The PDFs (33) and (34) are almost identical. As mentioned above this is the consequence of the small correlation among the coefficients a_ν and b_ν for the vast majority of the frequencies. Secondly, not unexpectedly, the sample distribution of the maxima of the LSP and the CP are very similar. Finally in the first two experiments, contrary to what has been found by Süveges et al. (2015) in another set of experiments, the PDF computed by means of Eq. 9 overperforms the approach by Baluev (2008), whereas the reverse holds for the third experiment. In this last case, however, the better approximation concerns only the left tail, whereas the right tail (the most important for the estimation of the SPFA) are similar. This is the consequence of the fact that the approach based on the extreme value theory provides only an upper limit to the SPFA and

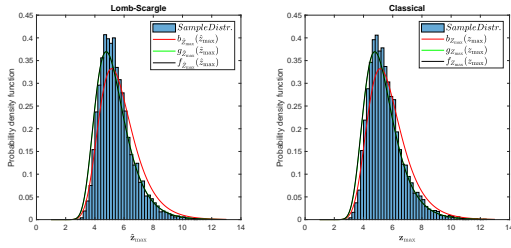


Figure 9. Histogram of the greatest peak for both the LSP and the CP obtained from 5000 numerical simulations of the experiment in Fig. 6 when the time series contains only a zero-mean, unit-variance white noise. The PDF $b_{z_{\max}}(z_{\max})$ derived from the extreme value theory by Baluev (2008), the PDF $g_{z_{\max}}(z_{\max})$ based on the exponential distribution given by Eq. (33) and the proposed PDF $f_{z_{\max}}(z_{\max})$ given by Eq. (34) are also plotted.

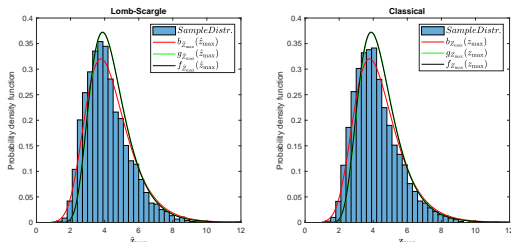


Figure 10. Histogram of the greatest peak for both the LSP and the CP obtained from 5000 numerical simulations of the experiment in Fig. 11 when the time series contains only a zero-mean, unit-variance white noise. The PDF $b_{z_{\max}}(z_{\max})$ derived from the extreme value theory by Baluev (2008), the PDF $g_{z_{\max}}(z_{\max})$ based on the exponential distribution given by Eq. (33) and the proposed PDF $f_{z_{\max}}(z_{\max})$ given by Eq. (34) are also plotted.

it requires that the LSP is free from strong aliasing effects. This condition is not satisfied in the present experiments.

6 APPLICATION TO AN ASTRONOMICAL TIME SERIES

As a comparison of the performance of two methods in real experimental situations, the proposed procedures are applied to the time series (standardized to zero-mean and unit-variance) in the top-left panel of Fig. 13. This time series is characterized by a rather irregular sampling. It was obtained with the VLA array (Biggs 1999) and consists of polarisation position angle measurements at an observing frequency of 15 GHz for one of the images of the double gravitational lens system B0218+357. The corresponding CP and LSP are shown in the top-right panel of Fig. 13. They have been computed on a set of 45 frequencies in the range $[0, 0.5]$ in unit of the Nyquist frequency (this last estimated on the basis of the shortest time distance between two observations). The similarity of the two periodograms is apparent. As explained above, this is due to the fact that, as it is visible in the bottom-left panel of Fig. 13, $|\rho_{\nu}|$ is small for all the frequencies. A prominent peak of amplitude ≈ 9.6 appears at $\nu = 1.37 \times 10^{-2}$ in both periodograms. The correlation matrix Σ shown in the bottom-right panel of the same figure results of full rank, hence $N^* = 45$ and the SPFAs as computed by means of Eqs. (9) for both the CP and the LSP are 6.5×10^{-3} and 2.8×10^{-3} , respectively. As expected, they are of the same order of magnitude.

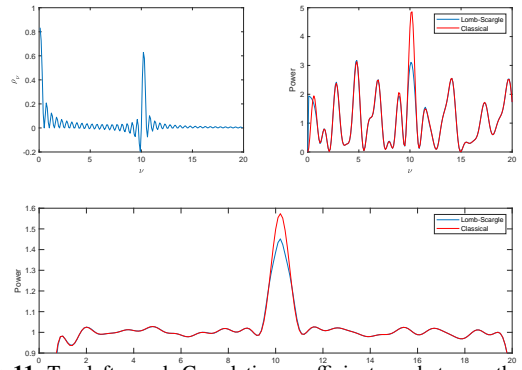


Figure 11. Top-left panel: Correlation coefficients ρ_{ν} between the coefficient a_{ν} and b_{ν} for the periodogram of a zero-mean, unit-variance, Gaussian, white-noise process added with a sinusoidal signal of frequency $\nu = 10.2$ and amplitude set to 0.15, sampling time grid identical to that used in Figs. 1 and 2 and computed on 200 frequencies uniformly distributed in the range $[0, 20]$. The frequency of the sinusoid corresponds to the frequency of the CP with the greatest correlation coefficients ρ_{ν} (see text). Top-right panel: corresponding Lomb-Scargle and CP. In the Lomb-Scargle periodogram it is visible the lowering of the highest peak with respect to the other peaks which makes it indistinguishable from the noise. Bottom-panel: mean of the Lomb-Scargle and CP obtained from 5000 time series with the same characteristics of the time series used in the top-right panel.

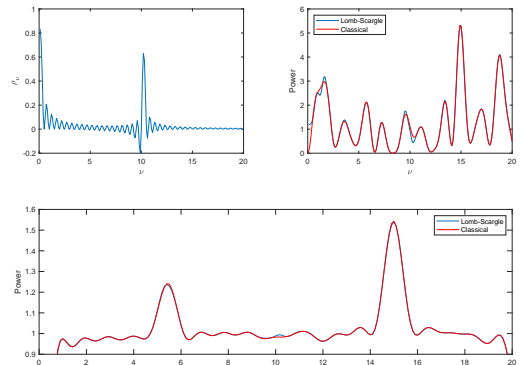


Figure 12. The same as in Fig. 11 but with a sinusoidal signal of frequency $\nu = 15.0$ and amplitude again set to 0.15. This frequency is characterized by a correlation coefficient $\rho_{\nu} \approx 0$. Contrary to the previous figure, here the Lomb-Scargle and CP are almost indistinguishable.

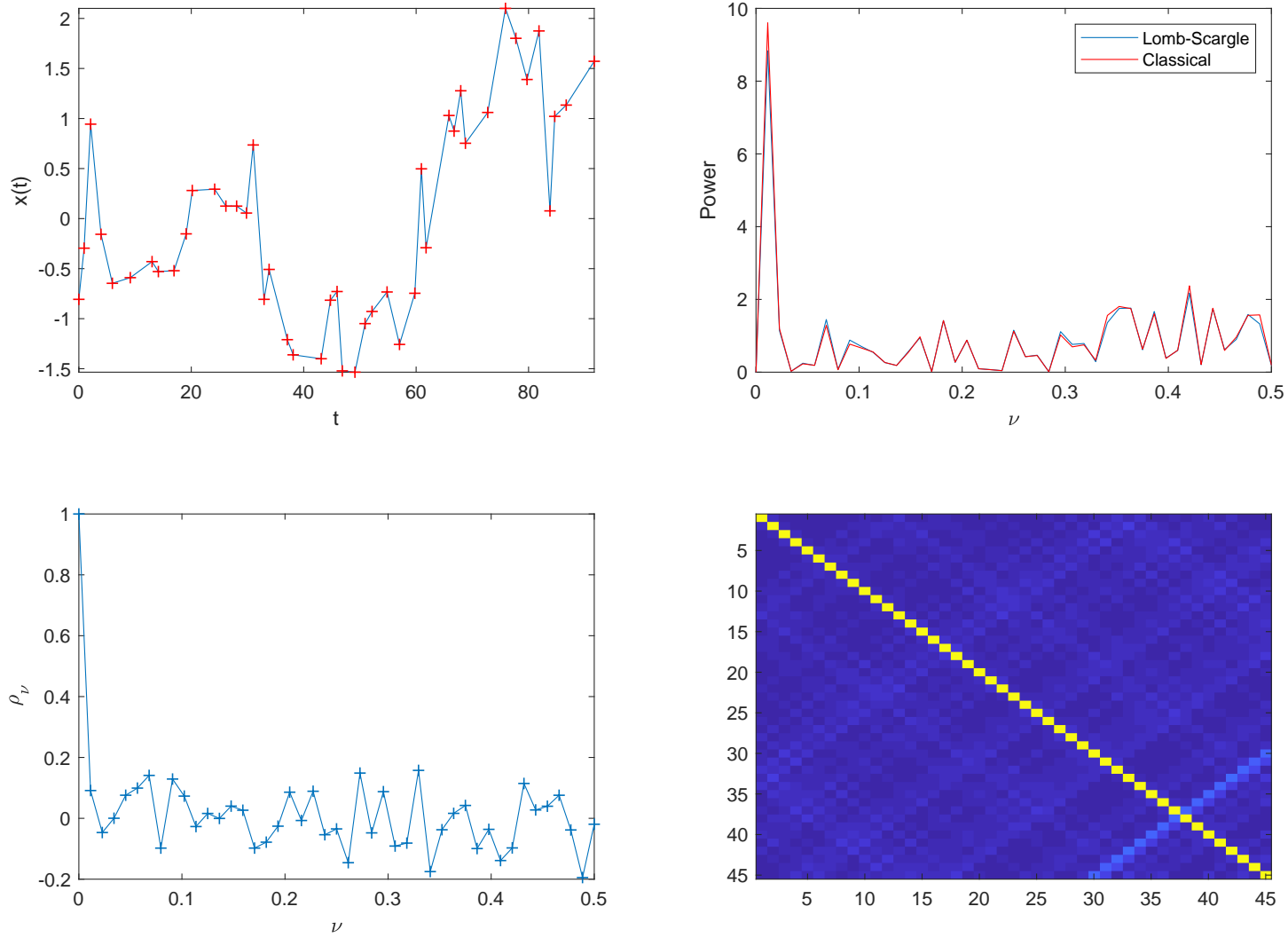


Figure 13. Top-left panel: experimental time series (standardized to zero mean and unit variance) containing 45 unevenly-spaced data from Biggs (1999). Top-right panel: corresponding classical and Lomb-Scargle spectrograms computed on 45 evenly spaced frequencies in the range $[0, 0.5]$ in units of the Nyquist frequency. Bottom-left panel: correlation coefficients ρ_ν between the coefficients a_ν and b_ν for the frequencies used in the periodogram. Bottom-right panel: correlation matrix Σ for the frequencies used in the periodogram. This matrix is dominated by the diagonal entries and results of full rank. This indicates that all the frequencies are mutually uncorrelated.

7 CONCLUSIONS

The Lomb-Scargle periodogram (LSP) has achieved great popularity thanks to its alleged capability of providing a statistical solution to the problem of the detection of signals embedded in noise when the sampling is irregular. Actually, this approach is based on the arbitrary procedure of forcing the entries of the periodogram to share the same exponential distribution. The appealing benefit is that it is possible to access to a number of statistical tools for assessing the reliability of a detection which are not available otherwise. However, in this way some theoretical difficulties are introduced which make its use difficult in certain steps of the detection procedure (e.g. the computation of the spectral windows), in the development of specific algorithms to compute the periodogram itself and the fact that, as it has been shown here, under certain conditions some statistically significant detections can be lost with respect to the classical periodogram (CP). For these reasons, and because of the fact that typically the LSP and the CP provide almost identical results, there is no reason why the former should be considered superior to the latter.

ACKNOWLEDGEMENTS

REFERENCES

- Bagchi, S., & Mitra, S.K. 1999, The Nonuniform Discrete Fourier Transform and Its Applications in Signal Processing (New York: Springer Sciences + Business Media)
- Baluev, R.V. 2008, MNRAS, 385, 1279
- Baluev, R.V. 2014, Astrophysics, 57, 434
- Biggs, A.D., Browne, I.W.A., Helbig, P., Koopmans, L. V. E., Wilkinson, P. N., Perley, R. A. 1999, MNRAS, 304, 349
- Björck, Å. 1999, Numerical Method for Least Squares Problems (Philadelphia: SIAM)
- Deeming, T.J. 1975, Ap. Space. Sci., 36, 137
- Gottlieb, E.W., Write, E.L., & Liller, W. 1975, ApJL 195, L33
- Hamming, R.W. 1973, Numerical Methods For Scientists and Engineering (New York: Dover)
- Helstrom, C.W. 1968, Statistical Theory of Signal Detection (Oxford: Pergamon Press)
- Hopkins, A.M., Miller, C.J., & Connolly, A.J. 2002, AJ, 123, 1086
- Horne, J.H., & Baliunas, S.L. 1986, ApJ, 302, 757
- Lehmann, E.L., & Romano, J.P., 2005, Testing Statistical Hypotheses (New York: Springer)
- Lomb, N.R. 1976, Ap. Space. Sci., 39, 447
- Miller, J.C., Genovese, C., Nichol, R.C. et al. 2001, AJ, 122, 3492
- Nuttal, A.H. 1972, Naval Underwater Systems Center, New London Lab., New London, Conn., Tech. Rep. 4297 (available at <https://apps.dtic.mil/dtic/tr/fulltext/u2/743066.pdf>)
- Potts, D., Steidl, G., & Tasche, M. 2001, in Modern Sampling Theory: Mathematics and Applications, Benedetto, J.J. & Ferreira, P.J.S.G. Eds. (New York: Springer Sciences + Business Media)
- Press, W.H., Teukolsky, S.A., Vetterling, W.T., & Flannery, B.P. 1992, Numerical Recipes in Fortran (Cambridge: Cambridge University Press)
- Reegen, P. 2007, A&A, 467, 1353
- Scargle, J.D. 1982, ApJ., 263, 835
- Shanker, P.M. 2017, Fading and Shadowing in Wireless Systems (New York: Springer)
- Suñeves, M. 2014, MNRAS, 440, 2114
- Suñeves, M., Guy, L.P., Eyer, L. et al. 2015, MNRAS, 450, 2052
- Simon, M.K. 2006, Probability Distributions Involving Gaussian Random Variables (New York: Springer)
- VanderPlas, J.T. 2018, ApJ Supp. Series, 236, 16
- Van Trees, H.L. 2001, Detection, Estimation and Modular Theory - Part I (New York: John Wiley & Sons)
- Vio, R., Andreani, & P., Biggs, A. 2010, A&A, 519, A85

- Vio, R., Diaz-Trigo, M., & Andreani, P. 2013, Astronomy and Computing, 1, 5
- Watkins, D.S. 2010, Fundamentals of Matrix Computations (Hoboken: John Wiley & Sons)
- Vityazev, V.V. 1996, Astron. & Astroph. Trans., 1996, 11, 139
- Vityazev, V.V. 1996, Astron. & Astroph. Trans., 1996, 11, 159
- Zechmeister, M., & KÄijrster, M. 2009, A&A, 496, 577
- Zhang, S., & Jin, J. 1996, Computation of Special Functions (New York: John Wiley & Sons)

APPENDIX A: WHY THE LOMB-SCARGLE PERIODOGRAM IS NOT BASED ON A CORRECT LEAST-SQUARES MODEL

Given an experimental uneven time series $\mathbf{x} = [x_{t_0}, x_{t_1}, \dots, x_{t_{M-1}}]$, testing the presence of an unknown signal $\mathbf{s} = [s_{t_0}, s_{t_1}, \dots, s_{t_{M-1}}]$ is based on the following assumptions:

(i) The signal is embedded in an additive noise \mathbf{n} , i.e. the time series \mathbf{x} is given by $\mathbf{x} = \mathbf{s} + \mathbf{n}$. Without loss of generality, it is assumed that $E[\mathbf{n}] = 0$, where $E[\cdot]$ denotes the expectation operator;

(ii) The noise \mathbf{n} is the realization of a stationary stochastic process here assumed to be of white type.

An approach based on the least-squares modeling can be adopted. In this case, if signal \mathbf{s} is unknown, it has to be assumed to have the form

$$s(t_j) = \sum_{k=0}^{N-1} [a_{\nu_k} \cos(2\pi\nu_k t_j) + b_{\nu_k} \sin(2\pi\nu_k t_j)], \quad (\text{A1})$$

with $j = 0, 1, \dots, M-1$. Of course, part of the coefficients $\{a_{\nu_k}\}$ and $\{b_{\nu_k}\}$ could actually be equal to zero. For example, this happens with periodic signals which are not pure sinusoids. However, in general this piece of information is not available in advance. As a consequence, assuming that the frequencies $\{\nu_k\}$ are fixed, the correct least-squares model for the estimation the coefficients $\{a_{\nu_k}\}$ and $\{b_{\nu_k}\}$ is ³

$$\begin{aligned} & \{[\tilde{a}_{\nu_k}, \tilde{b}_{\nu_k}]\} = \\ & \arg \min_{\{a_{\nu_k}, b_{\nu_k}\}} \left\{ \sum_{j=0}^{M-1} \left[x(t_j) - \sum_{k=0}^{N-1} [a_{\nu_k} \cos(2\pi\nu_k t_j) - b_{\nu_k} \sin(2\pi\nu_k t_j)] \right]^2 \right\}. \end{aligned} \quad (\text{A2})$$

This means that all the coefficients $\{a_{\nu_k}\}$ and $\{b_{\nu_k}\}$ have to be simultaneously estimated. A detection can be claimed if any of these coefficients results statistically different from zero.

This model is different from that implicitly assumed by the LSP, i.e.

$$\begin{aligned} & \{[\bar{a}_{\nu_k}, \bar{b}_{\nu_k}]\} = \\ & \arg \min_{a_{\nu_k}, b_{\nu_k}} \left\{ \sum_{j=0}^{M-1} [x(t_j) - a_{\nu_k} \cos(2\pi\nu_k t_j) - b_{\nu_k} \sin(2\pi\nu_k t_j)]^2 \right\}. \end{aligned} \quad (\text{A3})$$

It corresponds to assume that \mathbf{x} contains the contribution of one (and only one) pure sinusoidal signal \mathbf{s} of fixed frequency not due to the noise. Here, the point is that, for a given frequency ν_k , the

³ We recall that the function “ $\arg \min[H(x)]$ ” provides the value of x for which the function $H(x)$ has the smallest value.

coefficients \bar{a}_{ν_k} and \bar{b}_{ν_k} are identical to the corresponding \tilde{a}_{ν_k} and \tilde{b}_{ν_k} iff the set of sinusoidal functions constitutes an orthonormal basis (e.g. see [Hamming 1973](#), p. 450). This does not happen when the sampling is irregular. Hence, in most practical applications, the LSP is not based on the correct least-squares model.

APPENDIX B: NUMBER OF UNCORRELATED FREQUENCIES IN A PERIODOGRAM

In the case of an unequally spaced time series $\{x_{t_i}\}_{i=0}^{M-1}$ given by the realization of a discrete zero-mean, unit-variance, Gaussian white-noise process, the correlation ρ_{12} between the values of the periodogram in Eq. (1) at two frequencies ν_1 and ν_2 is given by ⁴,

$$\rho_{12} = \frac{\mathbb{E}[(a_1^2 + b_1^2 - \mu_{a_1^2} - \mu_{b_1^2})(a_2^2 + b_2^2 - \mu_{a_2^2} - \mu_{b_2^2})]}{\sqrt{\mathbb{E}[(a_1^2 + b_1^2 - \mu_{a_1^2} - \mu_{b_1^2})^2]} \sqrt{\mathbb{E}[(a_2^2 + b_2^2 - \mu_{a_2^2} - \mu_{b_2^2})^2]}}, \quad (\text{B1})$$

with $\mu_{a_i^2}$ and $\mu_{b_i^2}$ the expected values of a_i^2 and b_i^2 ,

$$\mu_{a_j^2} = \sum_{i=0}^{M-1} \cos^2(2\pi\nu_j t_i), \quad (\text{B2})$$

$$\mu_{b_j^2} = \sum_{i=0}^{M-1} \sin^2(2\pi\nu_j t_i). \quad (\text{B3})$$

When Eq. B1 is expanded, terms as

$$\mathbb{E}[a_1^2 a_2^2] = \sum_{i,j,l,m=0}^{M-1} \mathbb{E}[x_i x_j x_l x_m \cos(2\pi\nu_1 t_i) \cos(2\pi\nu_1 t_j) \times \cos(2\pi\nu_2 t_l) \cos(2\pi\nu_2 t_m)], \quad (\text{B4})$$

and similar ones must be evaluated considering four different situations, i.e. $i = j$ and $l = m$, $i = l$ and $j = m$, $i = m$ and $j = l$, and $i = j = l = m$. Keeping present this fact, after some algebra it is possible to show that

$$\rho_{12} = \frac{\varrho_{a_1 a_2}^2 \varrho_{a_1 b_2}^2 \varrho_{b_1 a_2}^2 \varrho_{b_1 b_2}^2}{\sqrt{\varrho_{a_1 a_1}^2 + \varrho_{b_1 b_1}^2 + 2\varrho_{a_1 b_1}^2} \sqrt{\varrho_{a_2 a_2}^2 + \varrho_{b_2 b_2}^2 + 2\varrho_{a_2 b_2}^2}}, \quad (\text{B5})$$

with

$$\varrho_{a_i a_n} = \sum_{i=0}^{M-1} \cos(2\pi\nu_i t_i) \cos(2\pi\nu_n t_i), \quad (\text{B6})$$

$$\varrho_{a_i b_n} = \sum_{i=0}^{M-1} \cos(2\pi\nu_i t_i) \sin(2\pi\nu_n t_i), \quad (\text{B7})$$

$$\varrho_{b_i a_n} = \sum_{i=0}^{M-1} \sin(2\pi\nu_i t_i) \cos(2\pi\nu_n t_i), \quad (\text{B8})$$

$$\varrho_{b_i b_n} = \sum_{i=0}^{M-1} \sin(2\pi\nu_i t_i) \sin(2\pi\nu_n t_i). \quad (\text{B9})$$

⁴ They assumption of $\sigma_n = 1$ for the white-noise process $\{x_{t_i}\}$ is not a limitation since ρ_{12} is independent of this parameter.

If the periodogram is compute on a set of N frequencies, from Eq. (B1) it is possible to construct the correlation matrix

$$\Sigma = \begin{pmatrix} \varrho_{11} & \varrho_{12} & \cdots & \varrho_{1(N-1)} & \varrho_{1N} \\ \varrho_{21} & \varrho_{22} & \cdots & \varrho_{2(N-1)} & \varrho_{2N} \\ \vdots & \vdots & \ddots & \vdots & \vdots \\ \varrho_{(N-1)1} & \varrho_{(N-1)2} & \cdots & \varrho_{(N-1)(N-1)} & \varrho_{(N-1)N} \\ \varrho_{N1} & \varrho_{N2} & \cdots & \varrho_{N(N-1)} & \varrho_{NN} \end{pmatrix}, \quad (\text{B10})$$

where $\varrho_{ii} = 1$ and $\varrho_{ij} = \varrho_{ji}$. Now, the correlation matrix Σ of a set of N uncorrelated random quantities is of full rank ⁵ (indeed, it is the identity matrix), i.e. $\text{rank}[\Sigma] = N$. Hence, if $\text{rank}[\Sigma] = N^*$, N^* provides the number of uncorrelated frequencies. Actually, strictly speaking, N^* computed in this way is not equivalent to the number of independent frequencies (uncorrelatedness does not imply independence). Indeed, in situations where $N > M$ it could happen that $N^* > M$, but this does not mean that the number of independent frequencies is N^* . This is because the number of independent frequencies can be as large as the number of degrees of freedom of the system (in this case the number of data) at most. Therefore, when $N^* > M$ the number of independent frequencies has to be assumed equal to M . In other words, M has to be intended as an upper limit to the number of independent frequencies.

Typically, the numerical computation of $\text{rank}[\Sigma]$ is based on the number of singular values ⁶ greater than a given tolerance tol . There are various choices to fix this quantity. An example is $tol = N\epsilon\|\Sigma\|_2$, where ϵ is the unit roundoff error ($= 2^{-52}$) and $\|\Sigma\|_2$ is given by the greatest singular values of Σ (see pag. 268 in [Watkins 2010](#)).

APPENDIX C: PDF AND CDF OF THE ENTRIES OF THE PERIODOGRAM OF A DISCRETE, UNEVEN, ZERO-MEAN, WHITE-NOISE PROCESS.

In the case of a discrete, uneven, zero-mean, white-noise process the PDF of the periodogram p , at a specific frequency is given by the PDF $f_Z(z)$ of the random variable $Z = X_1^2 + X_2^2$ with X_1 and X_2 zero-mean, Gaussian random variables with standard deviation σ_1 and σ_2 , respectively, and correlation coefficient ρ . This PDF can be obtained considering that Z can be expressed as the sum of two independent, squared, zero-mean, Gaussian random variables $\bar{X}_1 \sim \mathcal{N}(0, \bar{\sigma}_1^2)$ and $\bar{X}_2 \sim \mathcal{N}(0, \bar{\sigma}_2^2)$ with $\bar{\sigma}_1^2$ and $\bar{\sigma}_2^2$ the eigenvalues of the covariance matrix Σ of X_1 and X_2 ,

$$\Sigma = \begin{pmatrix} \sigma_1^2 & \rho\sigma_1\sigma_2 \\ \rho\sigma_1\sigma_2 & \sigma_2^2 \end{pmatrix}. \quad (\text{C1})$$

In formula,

$$\bar{\sigma}_1^2 = \frac{1}{2} \left(\sigma_1^2 + \sigma_2^2 - \sqrt{\sigma_1^4 + \sigma_2^4 + 2(2\rho^2 - 1)\sigma_1^2\sigma_2^2} \right), \quad (\text{C2})$$

$$\bar{\sigma}_2^2 = \frac{1}{2} \left(\sigma_1^2 + \sigma_2^2 + \sqrt{\sigma_1^4 + \sigma_2^4 + 2(2\rho^2 - 1)\sigma_1^2\sigma_2^2} \right). \quad (\text{C3})$$

Since $\bar{X}_i/\bar{\sigma}_i \sim \mathcal{N}(0, 1)$, it happens that $\bar{X}_i^2/\bar{\sigma}_i^2 \sim \chi_1^2$ with χ_1^2

⁵ The rank of a generic matrix \mathbf{A} , $\text{rank}[\mathbf{A}]$, is defined as the number of its linearly independent column vectors.

⁶ A generic $N \times N$ real matrix \mathbf{A} can always be factorized into the form $\mathbf{A} = \mathbf{U}\mathbf{D}\mathbf{V}^T$ where \mathbf{U} and \mathbf{V} are $N \times N$ orthogonal matrices, whereas \mathbf{D} is an $N \times N$ diagonal matrix whose diagonal elements $\delta_1 \geq \delta_2 \geq \dots \geq \delta_N \geq 0$ are known as singular values ([Björck 1996](#)).

the chi-squared distribution with one degree of freedom. In its turn, $\chi_1^2 = \Gamma(1/2, 2)$ with

$$\Gamma(a, b) = \begin{cases} \frac{b^a}{\Gamma(a)} \tau^{a-1} e^{-b\tau} & \text{if } \tau \geq 0, \\ 0 & \text{if } \tau < 0, \end{cases} \quad (\text{C4})$$

the Gamma PDF. Hence, $\bar{X}_i^2 \sim \bar{\sigma}_i^2 \Gamma(1/2, 2) = \Gamma(1/2, 2\bar{\sigma}_i^2)$. As a consequence, $f_Z(z)$ can be obtained by the convolution of two Gamma PDFs, $\Gamma(a_1, b_1)$ and $\Gamma(a_2, b_2)$,

$$f_Z(z) = \frac{b_1^{a_1} b_2^{a_2}}{\Gamma(a_1)\Gamma(a_2)} \int_0^z \exp[-b_1(z-y) - b_2 y] (z-y)^{a_1-1} y^{a_2-1} dy, \quad (\text{C5})$$

with $a_1 = a_2 = 1/2$, $b_1 = 1/(2\bar{\sigma}_1^2)$ and $b_2 = 1/(2\bar{\sigma}_2^2)$. The change of variable $y = zt$ provides

$$f_Z(z) = \frac{b_1^{a_1} b_2^{a_2} z^{a_1+a_2-1}}{\Gamma(a_1)\Gamma(a_2)} e^{-b_1 z} \int_0^1 \exp[(b_1 - b_2)zt] (1-t)^{a_1-1} t^{a_2-1} dt, \quad (\text{C6})$$

which can be written in the equivalent form

$$f_Z(z) = \frac{b_1^{a_1} b_2^{a_2} z^{a_1+a_2-1}}{\Gamma(a_1 + a_2)} e^{-b_1 z} {}_1F_1(a_2, a_1 + a_2; (b_1 - b_2)z), \quad (\text{C7})$$

with ${}_1F_1(\cdot, \cdot; \cdot)$ the Kummer confluent hypergeometric function. Finally, since

$${}_1F_1\left[\frac{1}{2}, 1; \gamma z\right] = \exp\left[\frac{\gamma z}{2}\right] I_0\left[\frac{\gamma z}{2}\right], \quad (\text{C8})$$

with $I_0(\cdot)$ the modified Bessel function of the first kind and zero order, and taking into account that in the present case

$$\gamma = \frac{\bar{\sigma}_2^2 - \bar{\sigma}_1^2}{2\bar{\sigma}_1^2 \bar{\sigma}_2^2}, \quad (\text{C9})$$

$f_Z(z)$ takes the form

$$f_Z(z) = \begin{cases} \exp\left[-\left(\frac{\bar{\sigma}_1^2 + \bar{\sigma}_2^2}{4\bar{\sigma}_1^2 \bar{\sigma}_2^2}\right)z\right] \frac{1}{2\bar{\sigma}_1 \bar{\sigma}_2} I_0\left[\frac{\bar{\sigma}_2^2 - \bar{\sigma}_1^2}{4\bar{\sigma}_1^2 \bar{\sigma}_2^2} z\right] & \text{if } z \geq 0, \\ 0 & \text{if } z < 0. \end{cases} \quad (\text{C10})$$

A useful approximation for $f_Z(z)$ can be obtained from the fact that for sufficiently great values of y , $I_0(y)$ can be well approximated by (Zhang & Jin 1996)

$$I_0(y) \approx \frac{e^y}{\sqrt{2\pi y}}. \quad (\text{C11})$$

Now, in the case of strongly correlated Gaussian random variable ($|\rho| \approx 1$), it happens that $\bar{\sigma}_2^2 \gg \bar{\sigma}_1^2 \approx 0$. Under this condition, it is possible to see that $f_Z(z)$, as given by Eq. (C10) with Eq. (C11), can be approximated by

$$f_Z(z) \approx \frac{1}{\bar{\sigma}_2 \sqrt{2\pi z}} e^{-z/(2\bar{\sigma}_2^2)}. \quad (\text{C12})$$

The CDF $F_Z(z)$ can be obtained by direct numerical integration of Eq. (C10) or by recognizing that, up to a constant $1/(2\bar{\sigma}_1 \bar{\sigma}_2)$, the required integral is of type $\int_0^z \exp(-pu) I_0(qu) du$ with solution given by Eq. (25) of the table of integrals in Nuttall (1972),

$$\int_0^z \exp(-pu) I_0(qu) du = \frac{1}{s} [1 + \exp(-pz) I_0(qz) - 2Q_1(v, w)], \quad p \neq q, \quad (\text{C13})$$

with $Q_1(\cdot, \cdot)$ the Marcum Q-function, $s = \sqrt{p^2 - q^2}$, $v = \sqrt{z(p-s)}$ and $w = \sqrt{z(p+s)}$. Here, $p = -(\bar{\sigma}_1^2 + \bar{\sigma}_2^2)/(4\bar{\sigma}_1^2 \bar{\sigma}_2^2)$ and $q = (\bar{\sigma}_2^2 - \bar{\sigma}_1^2)/(4\bar{\sigma}_1^2 \bar{\sigma}_2^2)$.